# SI Appendix for "Glacial weathering, sulfide oxidation, and global carbon cycle feedbacks"

by Mark Torres, Nils Moosdorf, Jens Hartmann, Jess Adkins, and A. Joshua West

## S1. Glacial data compilation

### S1.1. Database of glacial hydrology and weathering geochemistry

This study reports and analyzes a database containing stream chemistry data and spatial data of the contributing catchments (Figure S1). To identify relevant datasets, we searched the ISI Web of Knowledge and Google Scholar, using keywords related to glacier hydrochemistry and solute fluxes. The identified papers as well as their cited and citing articles defined the assessed body of published work on sub-glacial weathering and were scanned for published raw data. In total, about 50 texts reporting major ion concentrations or fluxes of glaciated catchments were collected. The reported values were combined in a Microsoft Excel table; details of the considered studies, sites, and data are provided in Datasets S1 and S2, and Tables S1 and S2. Some studies were not included in this compilation because they do not report numerical raw data (e.g., 1) or report no major ion chemistry (e.g., 2–4).

Where available, digital tables in spreadsheet format (available as online resources associated with the source article) were directly copied into a Microsoft Excel database (Dataset S1). Where digital spreadsheets were not available, data were copied electronically from article PDF files, or, if no digital copying was possible, the original data were input by hand. Input data were checked for plausibility and typing errors. In some cases, these checks revealed inconsistencies in the original data, which were corrected if possible and marked in the data table. In a few cases, inconsistencies led to omitting sources from the database, e.g., when a paper reported higher minimum than average values (5).

The analyses in this study are based on one single value per monitoring station and parameter. Where data from multiple times per site were provided, these values were averaged. Where possible, the average was discharge weighted. Our data analysis and interpretations focus on comparison of these average values between different catchments. As noted in the main text, solute concentrations and ratios within each individual catchment do vary with time, but this variability tends to be small, reflecting the "chemostatic" nature of hydrochemical systems (6), especially when compared to the differences between catchments. For example, catchments within our glacial database for which time series data were reported (e.g., 7) show percent-level changes in $SO_4$ to Na ratios over seasonal timescales, compared to the order-of-magnitude differences we observe between different catchments (Figure 2 of main text). Thus, although our analysis does not account for temporal variability, it is unlikely to bias our interpretations.

The contribution from chemical weathering to the measured stream chemistry was determined based on the mass-balance assumption that dissolved solids enter stream water only by chemical weathering and precipitation. In some cases, the original studies already corrected precipitation inputs, usually based on Cl normalized element ratios,

assuming all Cl originated from precipitation. These published corrections were used if available. If the source studies did not correct for precipitation inputs, the data were corrected using a representative chemical composition of rain, snowpack, or ice reported by the source studies. If no precipitation chemistry was provided for a catchment, data from a neighboring site was used. If no neighboring site seemed representative based on a visual assessment, regional datasets of precipitation chemistry were used (8, 9). In the few cases that no information on precipitation chemistry could be identified at a given site, precipitation was corrected with the average correction factors for the other 87 sites. The method of precipitation correction used for each site is listed in Dataset S1.

S1.2. Geospatial catchment characterization

Spatial representations of the sampling sites were defined in ESRI ArcGIS 10, based on coordinates, maps, or location descriptions provided in each source paper. Published coordinates were input directly. Maps or location descriptions were compared with Google Earth or Microsoft Bing (MS Bing) satellite imagery to identify a suitable representation of the sampling locations. For the location 'Fairchild2' (location IDs are identified in Dataset S1) a later publication from the same sampling campaign reported the sampling location (10).

Catchment boundaries were either automatically derived from a digital elevation model (DEM). ASTER GDEM Version 2 was used for Iceland, Svalbard and the Kilimanjaro, and SRTM Hydrosheds 15" (11) for the other areas. Sinks in the ASTER GDEM were filled using the "fill" tool of the ArcGIS Spatial Analyst. From the filled DEM, flow direction rasters and flow accumulation rasters were generated to calculate the catchments using the "watershed" tool of the Spatial Analyst. SRTM Hydrosheds already provided the necessary input layers for the "watershed" tool. For some rivers, a comparison between the catchment boundaries derived from the DEM flow routing and satellite imagery revealed obvious errors (e.g., the calculated catchment boundaries crossed a drainage divide), presumably due to errors in the elevation model. In these instances, the catchment boundaries were manually digitized using either the published location maps or MS Bing satellite imagery implemented in ArcGIS.

Data of glacial coverage within each catchment and the sampling distance from the glacier snout were taken from the original publications where possible, as these measurements are assumed to best reflect conditions at the time of sampling. If the glaciated area within a catchment was reported but not the catchment size, the size was determined in ArcGIS and used to calculate the glaciated proportion. If the original publication did not report the glaciated area within the catchment, we used the GLIMS database (12), which contains shapefiles for a large number of glaciers, along with the catchment boundaries from ArcGIS to calculate the glaciated area. For some rivers, the estimate of glacial cover using the GLIMS database was 0% despite the fact that the original publication reported a glacier in the catchment. We visually inspected satellite imagery (primarily via MS Bing) to identify each glacier and manually digitized its extent to determine the proportion of glaciated area. To check for consistency between the different measurements of glaciated area, we compared estimates from the original

publication, GLIMS, and MS Bing satellite imagery for all catchments (Figure S2). Expect in the cases where the glacier was missing from the GLIMS database, there is good agreement between the different measurement approaches (Figure S2). Locations from four studies where it was not possible to define glaciated areas were omitted (13–16). Data regarding the lithology of each catchment were taken from the global lithological map database (17).

In total, 95 glaciated catchments (Figure S1) provided at least 1 sample with concentrations of Ca, Mg, Na and K. These were included in the database. Measured discharge was available for 52 of these catchments. Spatial datasets of modelled runoff (18) are unsuitable to substitute for measured discharge in glaciated catchments because of the dependence of actual runoff on glacial meltwater, which is weakly represented in the models. However, in some locations, discharge data was derived from other publications focusing on the same location: 'Hasnain1' with runoff from (19), 'Kumar1' and 'Singh2' (both describing an identical location) with runoff from (20), and 'Wadham1' with runoff from (21). Because some parameters were unavailable for some catchments, the numbers of catchments included in individual analyses (e.g., correlations) can vary. All reported correlations in the text and tables of this study are Pearson-Rank correlations, because the input data are not normal distributed. Only significant ($p<0.05$) correlations are reported in the text.

## S2. Global River Chemistry (GloRiCh) Database

The GLObal RIver CHemistry database GLORICH combines hydrochemical data assembled from varying sources (Dataset S3), and adds newly calculated catchment characteristics of the sampling locations (22). The information provided includes catchment size, lithology, soil, climate, land cover, net primary production, population density and average slope gradient. At present, the database comprises ~1.27 million samples distributed over 18,897 sampling locations from 15,516 catchments.

## S3. Tracing the effects of weathering on atmospheric $pCO_2$

The effect of chemical weathering on atmospheric $pCO_2$ can be deduced from the dissolved load of rivers by developing a framework for linking solute sources to the aqueous carbonate system that governs the partitioning of $CO_2$ between the atmosphere and ocean. Here, we make use of the fact that alkalinity and dissolved inorganic carbon (DIC) can uniquely define aqueous carbonate speciation at constant pressure, temperature, and salinity. Furthermore, alkalinity and DIC generally mix conservatively and can be tied directly to chemical weathering reactions. To first order, the $pCO_2$ of the ocean depends more on the ratio of alkalinity to DIC (Alk:DIC) than their absolute concentrations (Figure 3B). As a result, inferring the Alk:DIC of weathering reactions from the the solute chemistry of rivers provides a means to assess whether chemical weathering is a $CO_2$ source or sink over different timescales.

The generation of alkalinity and DIC by chemical weathering depends on which chemical reactions generate protons to drive weathering and which mineral phases consume these protons and liberate alkaline earth cations. Here, we consider weathering reactions where protons are generated from either the dissociation of carbonic acid or the oxidation of sulfide minerals and are used to drive the weathering of

either carbonate or silicate minerals. To quantify the relative generation of alkalinity and DIC by each of these reactions, we start by writing the relevant half-reactions and then combine them to yield the full reactions for the weathering of carbonate and silicate minerals by carbonic and sulfuric acids. The stoichiometries of the full reactions are then used to determine which combinations of reactions lead to variations in atmospheric $pCO_2$ over different timescales.

The half-reactions for acid generation by the disassociation of carbonic acid and the oxidation of pyrite can be written as:

$$H_2CO_3 \leftrightarrow H^+ + CO_3^{2-} \quad \text{(eq. S1)}$$

and

$$4FeS_2 + 15O_2 + 14\,H_2O \leftrightarrow 8SO_4^{2-} + 16H^+ + 4Fe(OH)_3 \quad \text{(eq. S2)}$$

Similarly, the half-reactions for the proton-promoted dissolution of carbonate and silicate minerals can be written as:

$$2H^+ + CaCO_3 \leftrightarrow Ca^{2+} + H_2CO_3 \quad \text{(eq. S3)}$$

and

$$4H^+ + CaSiO_4 \leftrightarrow 2Ca^{2+} + H_4SiO_4 \quad \text{(eq. S4)}$$

The above equations are combined with the assumption that the number of moles of protons generated and consumed should be equal. When combining the equations, we follow the convention of writing all species as the dominant species at the carbonic acid equivalence point. In particular, this means that we write all DIC species as $H_2CO_3$ and balance reactions by adding protons as needed. So, after canceling out species that appear on both sides of an equation, any $H_2CO_3$ that appears on the right hand side of an equation reflects DIC generation while any protons that appear on the left hand side of an equation reflect alkalinity production. This approach yields the full equations for carbonate weathering by carbonic acid:

$$2H^+ + CaCO_3 \leftrightarrow Ca^{2+} + H_2CO_3 \quad \text{(eq. S5)}$$

carbonate weathering by sulfuric acid:

$$0.5FeS_2 + \frac{15}{8}O_2 + \frac{7}{4}H_2O + CaCO_3 \leftrightarrow SO_4^{2-} + 0.5Fe(OH)_3 + Ca^{2+} + H_2CO_3 \quad \text{(eq. S6)}$$

silicate weathering by carbonic acid:

$$4H^+ + CaSiO_4 \leftrightarrow 2Ca^{2+} + H_4SiO_4 \quad \text{(eq. S7)}$$

and silicate weathering by sulfuric acid:

$$FeS_2 + \frac{15}{4}O_2 + \frac{7}{2}H_2O + CaSiO_4 \leftrightarrow 2SO_4^{2-} + Fe(OH)_3 + 2Ca^{2+} + H_4SiO_4 \quad \text{(eq. S8)}$$

Note that, as written, the equation for silicate weathering by carbonic acid does not explicitly include carbonic acid as a reactant. This is because the same number of moles of DIC (written as $H_2CO_3$ following the conventions listed above) appear on both the right and left hand sides of this equation and thus cancel out. So, while silicate weathering can be driven by carbonic acid, this reaction does not produce DIC.

To compare the effects of each full reaction on alkalinity and DIC generation independent of mineral stoichiometries, we normalize all reactions by the charge equivalents of cations released, which is the quantity shown in Figure 3A. This convention is particularly important for silicate minerals, which contain cations other than $Ca^{2+}$ (e.g., $Na^{+}$).

Using the moles of alkalinity and DIC generated per charge equivalent of cation released, the ratio of alkalinity to DIC generated by chemical weathering can be calculated from the relative contribution of each of the four full reactions to the cation budget. To develop a simple expression for Alk:DIC based on solute sources, we write separate mass balance equations for alkalinity and DIC using the full reactions listed above and take their ratio, which yields the equation:

$$\frac{Alk}{DIC} = \frac{(1-z) \times (x+y)}{(z \times 0.5x)+((1-z)\times 0.5x)} \quad \text{(eq. S9)}$$

where *y* is the fraction of cations from silicate weathering, *x* is the fraction of cations from carbonate weathering, and *z* is the proportion of protons sourced from sulfide mineral oxidation.

To use Equation S9 to assess the effect of weathering reactions on atmospheric $pCO_2$, it is useful to define threshold values of Alk:DIC that yield no change in $pCO_2$. The sign of deviations from this threshold ratio thus determine whether weathering acts a $CO_2$ source or sink. A value of 1 is a useful threshold Alk:DIC since the Alk:DIC of the modern ocean is approximately equal to 1 and $pCO_2$ is relatively constant at a fixed Alk:DIC (Figure 3). Setting Equation S9 equal to 1 and solving for *x*, *y*, and *z* yields the combinations of silicate and carbonate weathering by carbonic and sulfuric acid that are $pCO_2$ neutral. We find that the Alk:DIC generated by weathering is equal to 1 when

$$Z_{short} = 1 - (0.5 \times R) \quad \text{(eq. S10)}$$

where *R* is the proportion of cations sourced from carbonate weathering ($R = x / (x+y)$). We link the Alk:DIC = 1 threshold to "short" timescales since it does not take into account the fact that the removal of alkalinity and DIC from the ocean by carbonate mineral burial also affects the Alk:DIC of the ocean and, by extension, its $pCO_2$.

The export of alkalinity and DIC from the ocean as carbonate minerals can be incorporated into our framework by setting the threshold Alk:DIC equal to 2, which is the ratio associated with carbonate mineral precipitation (i.e., the reverse of equation 3). Solving Equation S9 for Alk:DIC = 2 yields the relationship:

$$Z_{long} = 1 - R \quad \text{(eq. S11)}$$

Equation S11 implies that weathering is $pCO_2$ neutral when it supplies alkalinity and DIC in the same ratio as they are removed from the ocean through carbonate precipitation provided that the input and output fluxes of alkalinity and DIC are equal.

In summary, if the proportions of carbonate and silicate weathering by carbonic and sulfuric acid yield Alk:DIC < 1, weathering is a $CO_2$ source. If weathering yields an Alk:DIC greater than 1 but less than 2, weathering is a $CO_2$ source over the timescale of carbonate burial in the ocean. If weathering yields an Alk:DIC > 2, weathering is a $CO_2$ sink. The Alk:DIC of weathering can be calculated from the proportion of cations sourced from carbonate versus silicate mineral weathering (*R*) and the proportion of these cations liberated via sulfuric acid weathering (*z*). These proportions can be inferred from the solute chemistry of rivers using an end-member mixing model, which is described in the following section.

## S4. Mixing model and calculation of Alkalinity:DIC ratios of weathering

To understand the effects of chemical weathering on atmospheric $CO_2$ using the Alk:DIC framework described above, it is necessary to apportion the budgets of major elements between all sources that contribute solutes (23–27). We consider (1) silicate mineral dissolution, (2) carbonate mineral dissolution, (3) evaporite dissolution, (4) sulfide mineral oxidation, and (5) atmospheric deposition as sources of dissolved Cl, $SO_4$, Na, K, Ca, and Mg. To quantitatively partition these solutes between their sources, we combine three distinct approaches to account for the budgets of (1) Cl, Na, Ca, and Mg, (2) $SO_4$, and (3) K, respectively. Importantly, the three approaches are inter-dependent so that the contributions from a solute source derived from one of the models will not conflict with the contributions predicted by the others for the same set of calculations on a single sample. Below, the details of our three model approaches are described in more detail.

### S4.1. Apportionment of Cl, Na, Ca, and Mg budgets

We apportion the Cl, Na, Ca, and Mg budgets by inverting the general end-member mixing equation:

$$X_{\mathrm{riv}} = \sum_{i=1}^{n} F_i \times X_i \qquad \text{(Eq. S12)}$$

where $X_{riv}$ is the tracer composition measured in a river water sample, $X_i$ is the tracer composition of the $i^{th}$ end-member, and $F_i$ is the fractional contribution of the $i^{th}$ end-member to the tracer budget, and n is the number of end-members. Following previous approaches (23, 27, 28), we use Na-normalized elemental ratios as mixing tracers. Since the fractional contribution of each end-member must sum to one, this approach yields 4 equations.

With 4 equations and 5 end-members (see above), it is not possible to consider all of our end-members using this approach. However, since sulfide mineral oxidation does not directly contribute to the budgets of Cl, Na, Ca, or Mg, it can initially be ignored as an end-member so that the number of equations exactly matches the number of

unknowns (i.e., the fractional contributions from carbonate, silicate, evaporite, and atmospheric end-members).

To parametrize the mixing model, it is necessary to assign values for the Na-normalized elemental ratios of each of the four end-members. While it is likely that there is a "true" value for the elemental ratio composition of each end-member for each sample (i.e., for each catchment in our database), these "true" values are unknown. Instead, we define ranges of elemental ratios that account for known variations in the composition of each end-member. We select these *a priori* ranges for each end-member based on published literature and expected mineral stoichiometries (Figure 2B, main text). The values used for each end-member are shown in Table S4 and are described in more detail below for selected elements.

In order to account for variable end-member ratios, we employ a Monte-Carlo routine where a solution to the system of mixing equations is calculated for different random combinations of end-member ratios. For each end-member ratio, we use a uniform distribution of values with a range equal to that shown in Table S4 and Figure 2B. For each sample, $10^4$ random values are drawn from each end-member distribution and used to parameterize the mixing equations. The exact number of random draws, or simulations, was selected in order to minimize variations in the 95% confidence interval of model results between replicate calculations. For each sample, some simulations produce negative values for the fractional contribution of one or more end-members. We treat these values as spurious and remove them from consideration for each sample.

S4.2. Apportionment of $SO_4$ budgets

In rivers, dissolved sulfate is sourced predominately from sulfide mineral oxidation, atmospheric deposition, and evaporite mineral dissolution. For both atmospheric deposition and evaporite mineral dissolution, the supply of dissolved $SO_4$ should be accompanied by the supply of dissolved Cl. Consequently, constraints on the Cl budget determined from the inversion model (Equation S12) can be used along with constraints on the $SO_4$ to Cl ratio of atmospheric deposition and evaporite weathering to constrain the $SO_4$ budget. In this way, the amount of sulfate sourced from sulfide mineral oxidation can be calculated as the difference between the total measured $SO_4$ concentration and the amount predicted from atmospheric and evaporite contributions.

To constrain the $SO_4$ to Cl ratio of atmospheric deposition, we use the range of values observed in direct measurements of precipitation. For evaporite mineral dissolution, we use mineral stoichiometries to constrain plausible variations. Since evaporites are dominantly composed of halite (NaCl) and gypsum ($CaSO_4 \cdot (H_2O)$), the Ca to Na ratio of the evaporite end-member used in the inversion model (Equation S12) should roughly correspond to the ratio of gypsum to halite in the evaporite deposit. Since both $SO_4$ and Cl are present in approximately 1 to 1 ratios with Ca and Na in gypsum and halite respectively, the Ca to Na ratio of the evaporite end-member constrains its $SO_4$ to Cl ratio.

The *a priori* ranges of end-member ratios allow some inversion model simulations to predict that evaporite dissolution and atmospheric deposition supply more dissolved $SO_4$ than is actually measured in each sample. We treat these values as spurious and remove them from consideration for each sample. In this way, the $SO_4$ budget places additional constraints on our apportionment of the Cl, Na, Ca, and Mg budgets.

S4.3. Apportionment of K budgets

Like Na, dissolved K can be sourced from silicate weathering, atmospheric deposition, and evaporite dissolution. However, incongruent dissolution (29) and biological uptake (30) complicate the partitioning of the dissolved K between its different sources. Generally, K makes up a small proportion of the total cation budget (median values of 2-3% for each of the databases). So, to be conservative about partitioning the dissolved K budget, we assume that all K is sourced from the dissolution of silicates. This will lead to a potential overestimation of the contribution of silicate weathering, which will make catchments more likely to sequester atmospheric $CO_2$.

S4.4. Calculating the Alkalinity to DIC ratio of weathering

The generation of alkalinity and DIC by chemical weathering occurs at a characteristic ratio set by (1) the proportion of cations sourced from carbonate weathering relative to the total sum of cations sourced by both carbonate and silicate weathering and (2) the portion of carbonate and silicate weathering driven by sulfuric acid relative to the total amount of carbonate and silicate weathering (26). Using our mixing model results, the proportion of carbonate weathering (R) can be calculated as:

$$R = \frac{(\mathrm{Ca}_c + \mathrm{Mg}_c)}{(\mathrm{Ca}_c + \mathrm{Mg}_c) + (\mathrm{Ca}_s + \mathrm{Mg}_s + \mathrm{Na}_s + \mathrm{K}_s)} \quad \text{(Eq. 13)}$$

where subscript “s” refers to cations sourced from silicates and subscript “c” refers to cations sourced from carbonates. Similarly, the proportion of sulfuric acid weathering (Z) can be calculated as:

$$\mathrm{Z} = \frac{(\mathrm{SO}_4)_{py}}{(\mathrm{Ca}_c + \mathrm{Mg}_c) + (\mathrm{Ca}_s + \mathrm{Mg}_s + \mathrm{Na}_s + \mathrm{K}_s)} \quad \text{(Eq. 14)}$$

where subscript “py” refers to sulfate sourced from the oxidation of sulfide minerals. For both equations 2 and 3, all concentrations are in units of charge equivalents. Following prior work (26), R and Z can be related to the alkalinity to DIC ratio of weathering via a mass balance of alkalinity and DIC where

$$\frac{\mathrm{Alkalinity}}{\mathrm{DIC}} = \frac{(1 - Z)}{0.5 \times \mathrm{R}} \quad \text{(Eq. 15)}$$

A consequence of our Monte-Carlo routine is that each sample will be associated with a distribution of possible alkalinity to DIC ratios. We fit each of these distributions to a kernel distribution to find the proportion of simulations that have an alkalinity to DIC ratio

that is less than a reference value (F(x)). This calculation is done only for rivers where the mixing model returns more than 10 acceptable simulations in order to yield a reasonable estimate of the distribution of alkalinity to DIC ratios.

Following our knowledge of the carbonate system (26; also see discussion above and in the main text), we select reference alkalinity to DIC ratios of 1 and 2 to characterize the effects of weathering on atmospheric $pCO_2$ over short and long timescales respectively. Since the "true" values for the elemental ratio composition of each end-member are unknown, our approach for summarizing the distribution of results (e.g., Figure 4) reflects the probability that weathering in a particular catchment is a source of $CO_2$ on both short and long timescales.

S4.5. Effect of gypsum-rich evaporites

Previous apportionments of solute budgets in global rivers have assumed that evaporite deposits always have more halite than gypsum. This contrasts with the observation that deposits of gypsum-rich evaporites are known to occur (31). Additionally, rivers with known evaporite contributions display a range of Ca to Na ratios consistent with the dissolution of gypsum-rich evaporite deposits (Figure 2B). To account for this range of possible end-member values, we broaden the range of Ca to Na ratios for the evaporite end-member relative to previous models (23, 27, 28) and perform our mixing calculations using different *a priori* ranges of evaporite Ca to Na ratios, comparing the distributions of model results (Figure 4).

For the global large river and GloRiCh databases, we find significant changes in the distribution of F(x) values as we increase the upper bound of the Ca to Na ratio of the evaporite end-member (Figure 4). For the glacial database, no significant changes are observed (Figure 4). In part, this difference results from the fact that samples in the global large river and GloRiCh databases tend to have higher concentrations of Cl relative to samples in the glacial database. When samples have high chloride concentrations, a high Ca to Na ratio of the evaporite end-member means that a greater proportion of the sulfate budget can be attributed to evaporite mineral dissolution. Since gypsum-rich evaporite deposits are known to exist and evaporite-impacted rivers can have high Ca to Na ratios (Figure 2B), we conclude that the wider range of evaporite end-member ratios used in this study is reasonable.

## S5. Role of catchment properties in setting glacial chemistry

Our analysis focuses on comparison between glaciated and unglaciated catchments, finding systematic differences between the two. We hypothesize that glaciation itself is the most likely explanation for these differences, associated with glacial increases in erosion rates that increase the supply of highly reactive sulfide and carbonate phases. However, other catchment characteristics may differ between the glaciated and unglaciated databases. We have evaluated the effect of these here.

S5.1. Catchment areas

Relative to the world's largest rivers, rivers within our glacial database have smaller catchment areas (Figure S3A). The GloRiCh database samples the widest range of catchment areas, encompassing the full range of areas in both the world river and glacial river datasets (Figure S3A). To test whether comparing rivers with different catchment areas affects our results, we sub-sampled the GloRiCh database to select rivers with the same range of catchment areas as the glacial river database. As observed in the full dataset, the ratio of sulfate to sodium is significantly different between the glacial rivers and the subset of the GloRiCh rivers with the same range of catchment areas (Figure S3B). In part, this results from the fact that the neither the mean nor median $SO_4$:Na ratio depends on catchment area for the GloRiCh database. Instead, we observe the variance in the $SO_4$:Na ratio to decrease with increasing catchment area, which is consistent with self-averaging behavior. As a result, we conclude that comparing the distributions of $SO_4$:Na ratios between datasets with different ranges of catchment areas does not lead to any identifiable bias.

S5.2. Distance from glacial outlet and the influence of continued weathering of glacial debris

For the glaciated rivers, samples collected the farthest from the glacier (i.e. > 20 km for the snout) show a narrower range of $SO_4$:Na ratios relative to samples collected close to the glacier (Figure S3C). Similarly, further from the glacier, $SO_4$:Na ratios tend to be lower, but do not reach the lowest values of the full dataset (Figure S3C). This evidence for a weak dependence of $SO_4$:Na ratios on distance from the sampling snout may imply that the balance between sulfide mineral oxidation and silicate weathering changes with distance from the glacial either due to continued weathering of glacial sediments in the pro-glacial environment, or alternatively to incorporation of tributary sub-catchments dominated by fluvial weathering/erosion processes. However, the fact that $SO_4$:Na ratios are not correlated with the proportion of glaciated area in the catchment (Figure S3D) suggests that pro-glacial weathering does not systematically affect the balance between sulfide oxidation and silicate weathering. The disagreement between these two proxies (i.e. distance from snout and proportion of glaciated area) may be due to the fact that distance from the snout does not incorporate information about the catchment geometry. For example, rivers sampled at similar distances from the glacier can incorporate very different non-glacial areas depending on the aspect ratio of the catchment. As the proportion of glaciated area accounts for the catchment geometry, it is likely to better capture the relative importance of pro-glacial weathering in setting the balance between sulfide mineral oxidation and silicate weathering. Since $SO_4$:Na ratios do not vary with the proportion of glaciated area, we conclude that, at the scale considered in this study, continued weathering in the proglacial environment does not "erase" the signature of glacially-enhanced sulfide mineral oxidation.

If glacial material is exposed to weathering for sufficiently long amount of time, the fluxes from dissolution of glacially-sourced silicate minerals may outpace those from sulfide mineral oxidation due to the greater abundance of silicate minerals in most lithologies (e.g., 26). However, the extent to which glacial debris continues to weather may be limited. Indeed, glacially-derived sediments are often targeted in studies of the

composition of the continental crust due to their minimal degree of silicate weathering (32), highlighting the fact that much of the detritus produced by glacial weathering is not extensively weathered. Furthermore, many glaciated regions today are adjacent to the ocean, so a significant volume of glacial sediments is rapidly transported to marine depocenters with little additional chemical weathering. For example, estimates of the volume and age of glacial sediments deposited in marine basins off of Patagonia and the Antarctic Peninsula match erosion rates determined from thermochronometry (33), consistent with the hypothesis of the rapid transfer of glacial sediments out of the weathering zone.

S5.3. Catchment slope angle as a proxy for erosion rates

Previous work on sulfide mineral oxidation has suggested that the mass fluxes of sulfate derived from sulfide mineral oxidation increase with increasing erosion rate (34). Consistent with this relationship, we find that the $SO_4$/Na ratio of river catchments within the GloRiCh database increase with increasing mean catchment slope angle (Figure S4), which provides a first-order proxy for the catchment erosion rate (35). Potentially, this means that the elevated $SO_4$/Na ratios of glacial catchments may be due either to glacially-enhanced erosion rates or, alternatively, to a propensity for glaciers to be found in regions of otherwise elevated uplift and erosion rates. Since glacial erosion does not depend on slope angle in the same manner as fluvial erosion (36–38), and since we lack information about slope angles of glaciated catchments (i.e., beneath ice cover), it is not possible to use mean catchment slope angle to test whether the relationship between $SO_4$/Na ratios and erosion rates is the same for glacial and non-glacial catchments. Further targeted work will still be required to robustly identify the role of erosion as a causative versus coincidental factor setting the “unique” chemistry of glacial rivers. However, we emphasize that our interpretation that glaciers play an active role is consistent with the evidence for glacial enhancement of erosion (39) and the theory that sulfide oxidation is limited by material supply while silicate mineral weathering is generally not.

S5.4. Role of catchment lithology

The results shown in Figure 4 show that glacial rivers within our database have higher probabilities of being associated with $CO_2$ release (F(X)) relative to the world’s largest rivers. Specifically, for Alk:DIC < 2, we find that some of the glacial rivers have probabilities of as high as 80% while none of the world’s largest rivers return values this high. To check whether or not these glacial rivers sample a particular lithology, we re-displayed the data in Figure 4 as a stacked histogram where rivers are grouped based on their dominant lithology (Figure S5). Importantly, rivers with catchments dominated by each lithologic class (carbonate, metamorphic, plutonic, siliciclastic, and volcanic) span the full range of F(X) values. This suggests that the higher probability of glacial rivers being associated with $CO_2$ release is not due to the preferential sampling of glacial rivers underlain by a particular rock type.

## References cited in the SI Appendix text


1. Wadham JL, et al. (2010) Hydro-biogeochemical coupling beneath a large polythermal Arctic glacier: Implications for subice sheet biogeochemistry. *J Geophys Res* 115(F4):F04017.

2. Sharp M, Creaser RA, Skidmore M (2002) Strontium isotope composition of runoff from a glaciated carbonate terrain. *Geochim Cosmochim Acta* 66(4):595–614.

3. Arn K, et al. (2003) Strontium isotope systematics in two glaciated crystalline catchments: Rhone and Oberaar Glaciers (Swiss Alps). *Swiss Bull Mineral Petrol* 83(3):273–283.

4. Tipper ET, Lemarchand E, Hindshaw RS, Reynolds BC, Bourdon B (2012) Seasonal sensitivity of weathering processes: Hints from magnesium isotopes in a glacial stream. *Chem Geol* 312–313(0):80–92.

5. Ahmad S, Hasnain SI (2000) Meltwater Characteristics of Garhwal Himalayan Glaciers. *Geol Soc India* 56(4):431–439.

6. Godsey SE, Kirchner JW, Clow DW (2009) Concentration–discharge relationships reflect chemostatic characteristics of US catchments. *Hydrol Process* 23(13):1844–1864.

7. Bhatt MP, Masuzawa T, Yamamoto M, Sakai A, Fujita K (2000) Seasonal changes in dissolved chemical composition and flux of meltwater draining from Lirung Glacier in the Nepal Himalayas. *Debris-Cover Glaciers* (264):277–288.

8. Jeelani G, Bhat NA, Shivanna K, Bhat MY (2011) Geochemical characterization of surface water and spring water in SE Kashmir Valley, western Himalaya: Implications to water–rock interaction. *J Earth Syst Sci* 120(5):921–932.

9. NADP (2008) *National Atmospheric Deposition Program (NRSP-3)*.

10. Fairchild IJ, Killawee JA, Hubbard B, Dreybrodt W (1999) Interactions of calcareous suspended sediment with glacial meltwater: a field test of dissolution behaviour. *Chem Geol* 155(3-4):243–263.

11. Lehner B, Verdin K, Jarvis A (2008) New global hydrography derived from spaceborne elevation data. *EOS Trans* 89(10):93–94.

12. Armstrong R, et al. (2013) GLIMS glacier database. Available at: http://nsidc.org/glims/.

13. Axtmann EV, Stallard RF (1995) Chemical weathering in the South Cascade Glacier basin, comparison of subglacial and extra-glacial weathering. *Biogeochem Seas Snow-Cover Catchments* (228):431–439.

14. Wolff-Boenisch D, Gabet EJ, Burbank DW, Langner H, Putkonen J (2009) Spatial variations in chemical weathering and CO2 consumption in Nepalese High Himalayan catchments during the monsoon season. *Geochim Cosmochim Acta* 73(11):3148–3170.

15. Mckenzie JM, Mark BG, Thompson LG, Schotterer U, Lin PN (2010) A hydrogeochemical survey of Kilimanjaro (Tanzania): implications for water sources and ages. *Hydrogeol J* 18(4):985–995.

16. Chmiel S, Bartoszewski S, Siwek K (2011) Chemical denudation rates in the Wydrzyca catchment (Bellsund, Spitsbergen). *Ann Univ Mariae Curie-Sklodowska* 66(1):115.

17. Hartmann J, Moosdorf N (2012) The new global lithological map database GLiM: A representation of rock properties at the Earth surface. *Geochem Geophys Geosystems* 13(12):Q12004.

18. Fekete BM, Vorosmarty CJ, Grabs W (2002) High-resolution fields of global runoff combining observed river discharge and simulated water balances. *Glob Biogeochem Cycles* 16(3):1042.

19. Hasnain SI, Thayyen RJ (1999) Discharge and suspended-sediment concentration of meltwaters, draining from the Dokriani glacier, Garhwal Himalaya, India. *J Hydrol* 218(3–4):191–198.

20. Singh P, Haritashya UK, Kumar N, Singh Y (2006) Hydrological characteristics of the Gangotri Glacier, central Himalayas, India. *J Hydrol* 327(1–2):55–67.

21. Wadham JL, Hodson AJ, Tranter M, Dowdeswell JA (1996) The rate of chemical weathering beneath a quiescent, surge-type, polythermal-based glacier, southern Spitsbergen, Svalbard. *Ann Glaciol* 24:27–31.

22. Hartmann J, Lauerwald R, Moosdorf N (2014) A Brief Overview of the GLObal RIver Chemistry Database, GLORICH. *Procedia Earth Planet Sci* 10:23–27.

23. Gaillardet J, Dupré B, Louvat P, Allègre C (1999) Global silicate weathering and CO2 consumption rates deduced from the chemistry of large rivers. *Chem Geol* 159(1-4):3–30.

24. White AF, Bullen TD, Vivit DV, Schulz MS, Clow DW (1999) The role of disseminated calcite in the chemical weathering of granitoid rocks. *Geochim Cosmochim Acta* 63(13–14):1939–1953.

25. Spence J, Telmer K (2005) The role of sulfur in chemical weathering and atmospheric CO2 fluxes: Evidence from major ions, δ13CDIC, and δ34SSO4 in rivers of the Canadian Cordillera. *Geochim Cosmochim Acta* 69(23):5441–5458.

543 26. Torres MA, et al. (2016) The acid and alkalinity budgets of weathering in the
544 Andes–Amazon system: Insights into the erosional control of global
545 biogeochemical cycles. *Earth Planet Sci Lett*. doi:10.1016/j.epsl.2016.06.012.

546 27. Négrel P, Allègre CJ, Dupré B, Lewin E (1993) Erosion sources determined by
547 inversion of major and trace element ratios and strontium isotopic ratios in river
548 water: The Congo Basin case. *Earth Planet Sci Lett* 120(1):59–76.

549 28. Moon S, Chamberlain CP, Hilley GE (2014) New estimates of silicate weathering
550 rates and their uncertainties in global rivers. *Geochim Cosmochim Acta*
551 134(0):257–274.

552 29. Anderson SP, Drever JI, Humphrey NF (1997) Chemical weathering in glacial
553 environments. *Geology* 25(5):399–402.

554 30. Likens G, et al. (1994) The biogeochemistry of potassium at Hubbard Brook.
555 *Biogeochemistry* 25(2). doi:10.1007/BF00000881.

556 31. Melvin JL ed. (1991) *Evaporites, Petroleum and Mineral Resources* (Elsevier)
557 Available at: http://www.sciencedirect.com/science/article/pii/S0070457108702553
558 [Accessed July 12, 2016].

559 32. Gaschnig RM, et al. (2016) Compositional evolution of the upper continental crust
560 through time, as constrained by ancient glacial diamictites. *Geochim Cosmochim*
561 *Acta* 186:316–343.

562 33. Fernandez RA, et al. (2016) Latitudinal variation in glacial erosion rates from
563 Patagonia and the Antarctic Peninsula (46°S–65°S). *Geol Soc Am Bull* 128(5-
564 6):1000–1023.

565 34. Calmels D, Gaillardet J, Brenot A, France-Lanord C (2007) Sustained sulfide
566 oxidation by physical erosion processes in the Mackenzie River basin: Climatic
567 perspectives. *Geology* 35(11):1003 –1006.

568 35. Larsen IJ, Montgomery DR, Greenberg HM (2014) The contribution of mountains to
569 global denudation. *Geology*:G35136.1.

570 36. Bindschadler R (1983) The Importance of Pressurized Subglacial Water in
571 Separation and Sliding at the Glacier Bed. *J Glaciol* 29(101):3–19.

572 37. DiBiase RA, Whipple KX, Heimsath AM, Ouimet WB (2010) Landscape form and
573 millennial erosion rates in the San Gabriel Mountains, CA. *Earth Planet Sci Lett*
574 289(1–2):134–144.

575 38. Herman F, et al. (2015) Erosion by an Alpine glacier. *Science* 350(6257):193–195.

576 39. Herman F, et al. (2013) Worldwide acceleration of mountain erosion under a
577 cooling climate. *Nature* 504(7480):423–426.

40. Arendt A, et al. (2013) Randolph Glacier Inventory [v2.0]: A Dataset of Global Glacier Outlines.

41. Ehlers J, Gibbard PL, Hughes PD (2011) *Quaternary glaciations - extent and chronology : a closer look* (Elsevier, Amsterdam ; Boston).

**Supporting Information Tables (appended at the end of the SI Appendix)**

**Table S1.** List of catchments and details of source information for all catchments in the compilation presented in this study.

**Table S2.** Summary statistics for glaciated catchments by region, and comparison to literature values of global attributes.

**Table S3.** Spearman rank correlations of different analyzed parameters.

**Table S4.** Ranges of end-member values used in inversion model to determine source contributions.

**Supporting Information Datasets (uploaded as separate files, in xlsx and csv format)**

**Dataset S1.** Compiled data.

**Dataset S2.** References used in data compilation in Dataset S1.

**Dataset S3.** References used in the GloRiCh compilation.

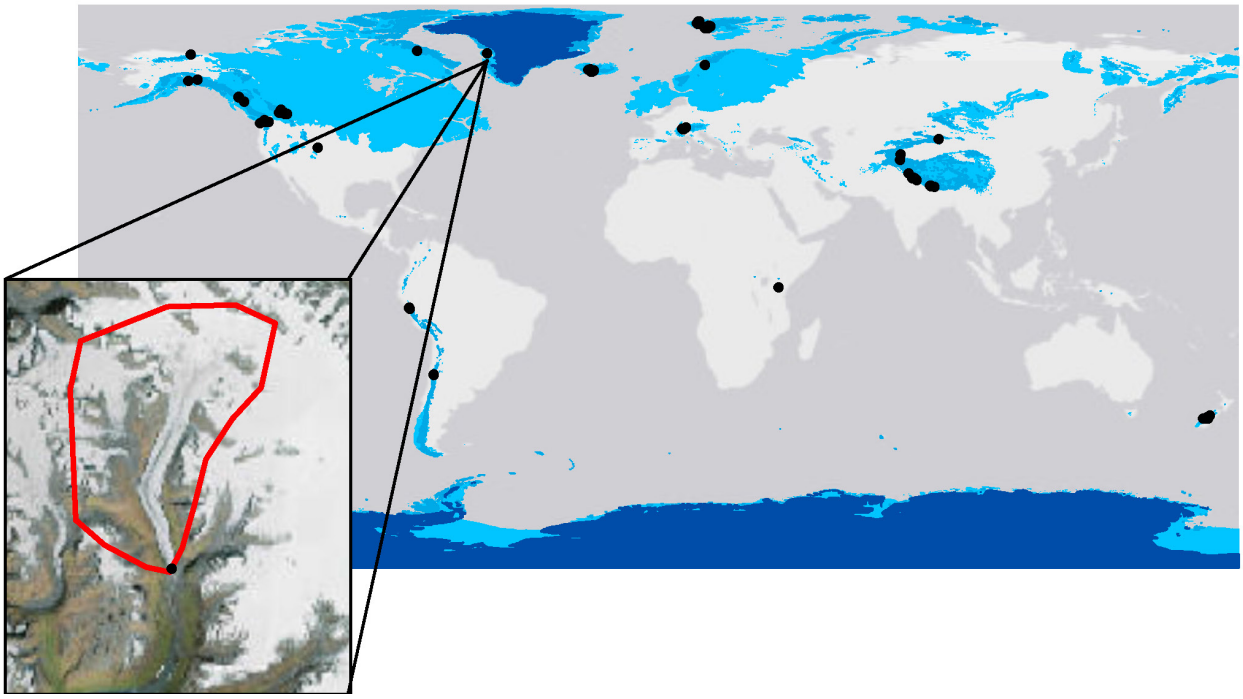

**Figure S1. Sampling localities for rivers in the glacial database.** World map showing the locations (black points) of the studies of glacial weathering in the new compilation presented here (Dataset S1), along with the extent of global ice cover today (darkest blue showing large ice sheets and medium blue alpine glaciers; 40) and at LGM (light blue; 41). Some location markers overlap. The inset shows satellite imagery of the Kuannersuit Valley, one example of a glacierized catchment. Data sources used in the process of mapping include Esri, HERE, DeLorme, MapmyIndia, @Openstreetmap contributors, the GIS user community, DigitalGlobe, GeoEye, i-cubed, USDA, USGS, AEX, Getmapping, Aerogrid, IGN, and IGP.

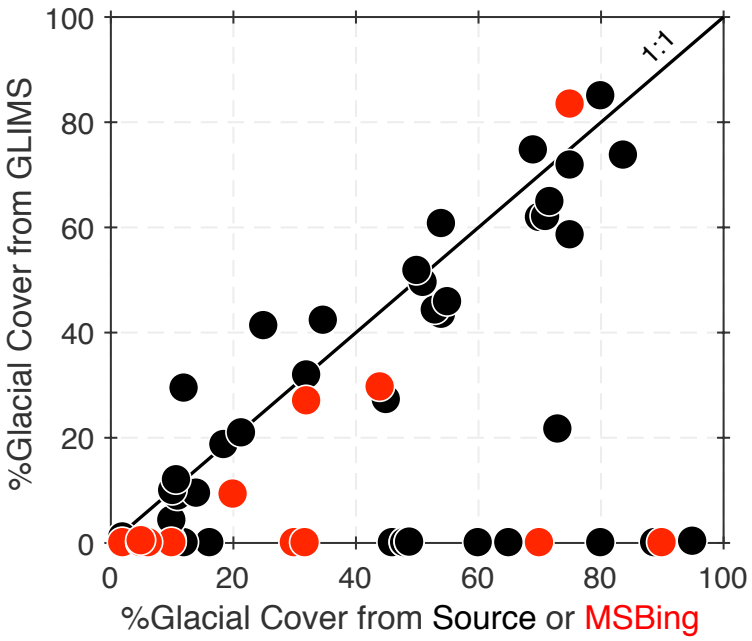


**Figure S2. Comparison of methods for determining glacial area.** Black circles compare the proportion of glaciated catchment area reported in the original publication (x-axis) with the proportion calculated using the GLIMS database (y-axis). Red circles compare the proportion of glaciated catchment area determined from MS Bing satellite imagery (x-axis) with the proportion calculated using the GLIMS database (y-axis). Except in cases where glaciers are missing from the GLIMS database, there is general agreement between the different approaches for estimating the proportion of glaciated catchment area.

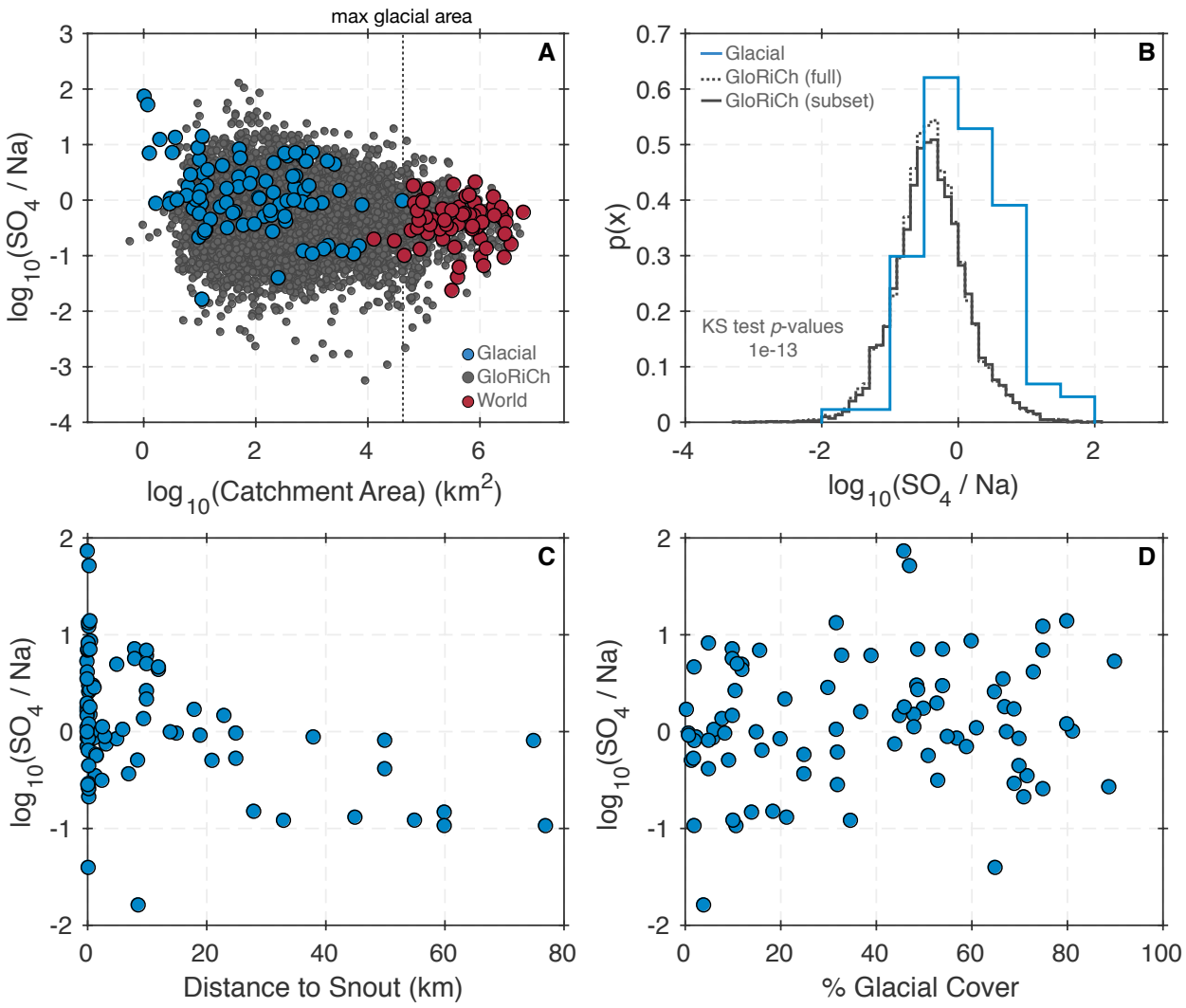


**Figure S3. Effects of catchment area, distance from glacier, and glaciated catchment area on sulfate to sodium ratios.** (A) The relationship between catchment area (x-axis) and sulfate to sodium ratio for rivers within the glacial (blue points), world's largest rivers (red points), and GloRiCh (grey points) databases. The dashed vertical line marks the largest catchment area in the glacial river database. (B) Comparison between the distributions of sulfate to sodium ratios for rivers from the glacial rivers (blue line) and GloRiCh databases (gray lines). The dashed grey line is the distribution for the full GloRiCh database while the solid gray line is the subset of GloRiCh catchments with the same range of catchment areas as the glacial database. A two-way KS test between the glacial rivers and the subset of the GloRiCh database suggests that the two datasets were not drawn from the same underlying distribution of values (*p*-value = $10^{-13}$). (C) Relationship between distance from the sampling site to the glacial snout (x-axis) and the dissolved sodium to sulfate ratio (y-axis). (D) Relationship between the percentage of glaciated catchment area (x-axis) and the dissolved sodium to sulfate ratio (y-axis).

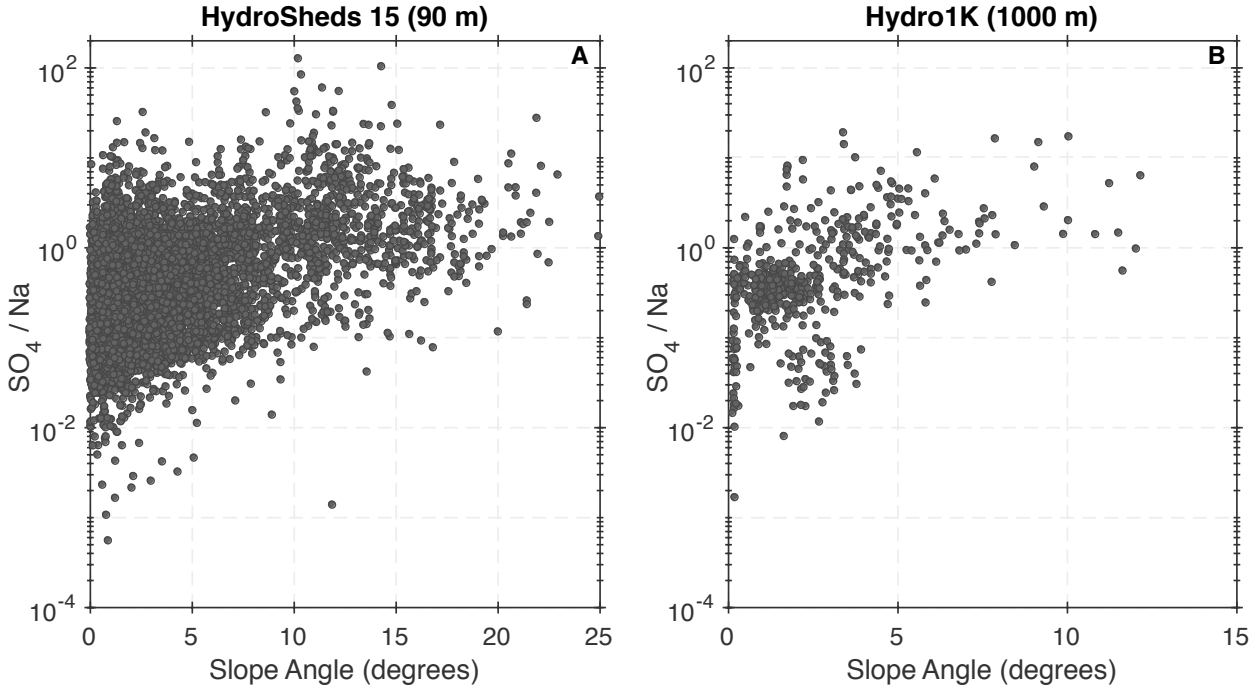


**Figure S4. Relationship between mean catchment slope angle and sulfate to sodium ratios for the GloRiCh database.** (A) Mean catchment slope angles calculated using the HydroSheds 15 digital elevation model (DEM) with a resolution of 90 m. (B) Mean catchment slope angles calculated using the Hydro1K DEM with a resolution of 1000 m.

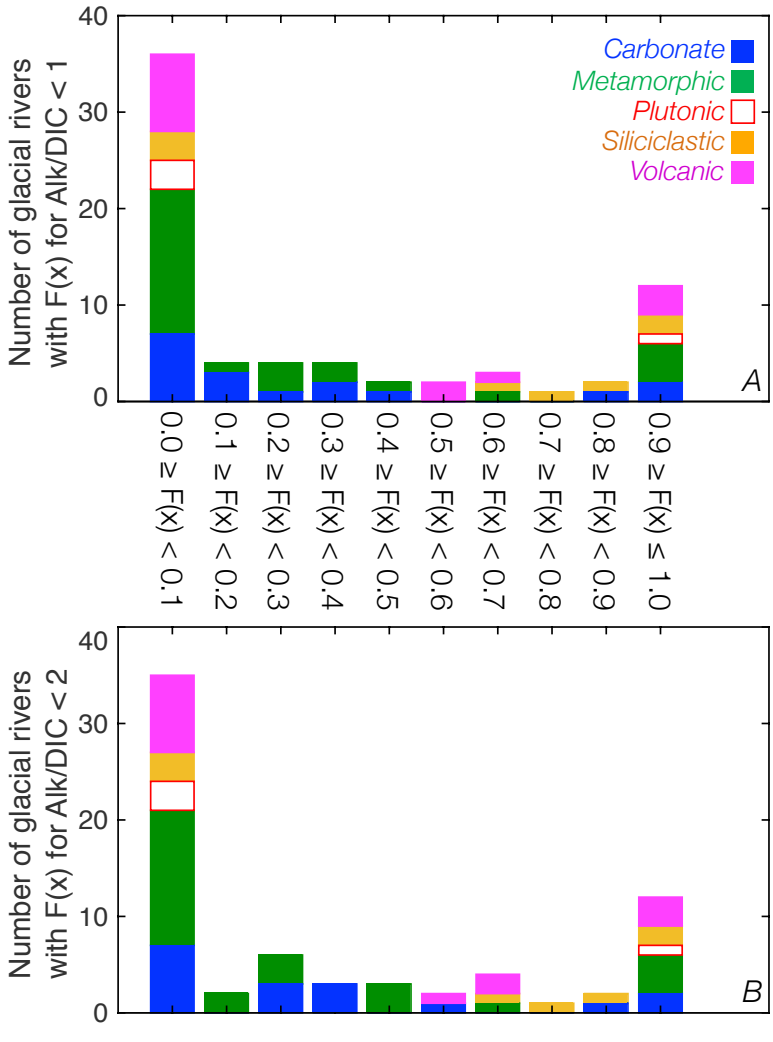


**Figure S5. Role of lithology in setting $CO_2$ release potential of glacial rivers.** Number of catchments in the glacial compilation that yield a proportion of model simulations, F(x), with Alk:DIC < 1 (panel A) or < 2 (panel B), classified by the predominant lithology class for each catchment.

Table S1: List of catchments and details of source information for all catchments in the compilation presented in this study.

| Catchment ID | Location | Watershed Method[1] | Region | Number of samples | Reference |
|---|---|---|---|---|---|
| Anderson1 | Kennicott River, Alaska | Hand | North | 150 | (Anderson et al., 2003) |
| Anderson2 | Bench river | Hand | North | 5 | (Anderson et al., 2000) |
| Axtmann1 | South Cascade Glacier, Stream 2 | Hand | Rocky Mountains | 24 | (Axtmann and Stallard, 1995) |
| Bhatt1 | Lirung Glacier | Hydrosheds | Himalaya | 39 | (Bhatt et al., 2000) |
| Chauhan1 | Satopanth & Bhagirath Kharak Glaciers | Hydrosheds | Himalaya | 17 | (Chauhan and Hasnain, 1993) |
| Chmiel1 | Scott River | Hand | North | 30 | (Chmiel et al., 2012) |
| Church1 | Lewis River | Hand | North | 19 | (Church, 1974) |
| Collins1 | Dornergetscher | Hydrosheds | Alps | 169 | (Collins, 1979) |
| Eyles1 | Berendon Watershed | Hydrosheds | Rocky Mountains | 2 | (Eyles et al., 1982) |
| Fairchild1 | Saskatchewan Glacier | Hydrosheds | Rocky Mountains | 12 | (Fairchild et al., 1994) |
| Fairchild2 | Tsanfleuron Glacier | Hand | Alps | 15 | (Fairchild et al., 1994) |
| Feng1 | Urumqi Glacier No.1 station | Hand | Himalaya | 217 | (Feng et al., 2012) |
| Fortner1 | Station Nr 5 | Hydrosheds | Andes | 1 | (Fortner et al., 2011) |
| Fortner2 | Station Nr 9 | Hydrosheds | Andes | 1 | (Fortner et al., 2011) |
| Fortner3 | Station Nr 10 | Hydrosheds | Andes | 1 | (Fortner et al., 2011) |
| Fortner4 | Station Nr 14 | Hydrosheds | Andes | 1 | (Fortner et al., 2011) |
| Gislason1 | THJORSA | Aster | Iceland | 23 | (Gislason et al., 1996) |
| Gislason2 | ÖLUFSA | Aster | Iceland | 23 | (Gislason et al., 1996) |
| Gislason3 | Hvita-s Gullfoss | Aster | Iceland | 23 | (Gislason et al., 1996) |
| Gislason4 | Tungufljot | Aster | Iceland | 23 | (Gislason et al., 1996) |
| Gislason5 | Sog | Aster | Iceland | 23 | (Gislason et al., 1996) |
| Gislason6 | HVITA-W, FERJUKOT | Aster | Iceland | 23 | (Gislason et al., 1996) |
| Gislason7 | Hvita-W, Kljafoss | Aster | Iceland | 23 | (Gislason et al., 1996) |
| Hasnain1 | Dokriani glacier, Ganga basin | Hydrosheds | Himalaya | 28 | (Hasnain and Thayyen, 1999b) |
| Hasnain2 | Eastern Lahul Valley | Hydrosheds | Himalaya | 37 | (Hasnain et al., 1989) |
| Hindshaw1 | Damma Glacier, Station A | Hydrosheds | Alps | 15 | (Hindshaw et al., 2011) |
| Hindshaw2 | Damma Glacier, Station B | Hydrosheds | Alps | 5 | (Hindshaw et al., 2011) |
| Hindshaw3 | Damma Glacier, Station E | Hydrosheds | Alps | 6 | (Hindshaw et al., 2011) |
| Hodgkins1 | Scott Turnerbreen | Aster | North | 72 | (Hodgkins et al., 1997) |

| | | | | | |
|---|---|---|---|---|---|
| Hodson1 | 1. Austre Brøggerbreen, Upper Site | Aster | North | 75 | (Hodson et al., 2000) |
| Hodson2 | 2. Austre Brøggerbreen, Lower Site | Aster | North | 110 | (Hodson et al., 2000) |
| Hodson3 | 5. Erdmannbreen, 1996 | Aster | North | 36 | (Hodson et al., 2000) |
| Hodson4 | 6. Midre Love´nbreen | Hand | North | 120 | (Hodson et al., 2000) |
| Hodson5 | 8. Hannabreen | Aster | North | 44 | (Hodson et al., 2000) |
| Hodson6 | 8. Erikbreen | Hand | North | 15 | (Hodson et al., 2000) |
| Hodson7 | Batura Glacier | Hydrosheds | Himalaya | 15 | (Hodson et al., 2002) |
| Hosein1 | Rhone | Hand | Alps | 76 | (Hosein et al., 2004) |
| Hosein2 | Oberaar | Hydrosheds | Alps | 52 | (Hosein et al., 2004) |
| Jacobson1 | Hooker | Hydrosheds | New Zealand | 1 | (Jacobson et al., 2003) |
| Jacobson2 | Tasman | Hydrosheds | New Zealand | 1 | (Jacobson et al., 2003) |
| Jacobson3 | Jolle | Hydrosheds | New Zealand | 1 | (Jacobson et al., 2003) |
| Jacobson4 | Cass | Hydrosheds | New Zealand | 1 | (Jacobson et al., 2003) |
| Jacobson5 | Waiho | Hydrosheds | New Zealand | 1 | (Jacobson et al., 2003) |
| Jacobson6 | Fox | Hydrosheds | New Zealand | 1 | (Jacobson et al., 2003) |
| Jacobson7 | Cook | Hydrosheds | New Zealand | 1 | (Jacobson et al., 2003) |
| Jacobson8 | Karangarua | Hydrosheds | New Zealand | 1 | (Jacobson et al., 2003) |
| Krawczyk1 | Bayelva basin | Aster | North | 42 | (Krawczyk et al., 2003) |
| Krawczyk2 | Scottbreen | Hand | North | 60 | (Krawczyk and Bartoszewski, 2008) |
| Kumar1 | Gangotri Glacier | Hydrosheds | Himalaya | 21 | (Kumar et al., 2009) |
| Lecomte1 | M1 | Hydrosheds | Andes | 10 | (Lecomte et al., 2008) |
| Lecomte2 | M3 | Hydrosheds | Andes | 1 | (Lecomte et al., 2008) |
| Lecomte3 | M4 | Hydrosheds | Andes | 2 | (Lecomte et al., 2008) |
| Lecomte4 | M6 | Hydrosheds | Andes | 1 | (Lecomte et al., 2008) |
| Lecomte5 | M9 | Hydrosheds | Andes | 2 | (Lecomte et al., 2008) |
| Lyons1 | Hokitika | Hydrosheds | New Zealand | 17 | (Lyons et al., 2005) |
| Lyons2 | Fox | Hydrosheds | New Zealand | 1 | (Lyons et al., 2005) |
| Lyons3 | Haast | Hydrosheds | New Zealand | 7 | (Lyons et al., 2005) |
| Lyons4 | Karangarua | Hydrosheds | New Zealand | 1 | (Lyons et al., 2005) |
| Lyons5 | Waiho | Hydrosheds | New Zealand | 1 | (Lyons et al., 2005) |
| Mark1 | YAN | Hand | Andes | 14 | (Mark and Seltzer, 2003) |
| Mckenzie1 | 17 Lion River | Aster | Kilimanjaro | 1 | (Mckenzie et al., 2010) |

| | | | | | |
|---|---|---|---|---|---|
| Moosdorf1 | 102637 | Hydrosheds | Rocky Mountains | 37 | (Moosdorf et al., 2011b) [A)] |
| Moosdorf2 | 102689 | Hydrosheds | Rocky Mountains | 72 | (Moosdorf et al., 2011b) [A)] |
| Moosdorf3 | 102690 | Hydrosheds | Rocky Mountains | 30 | (Moosdorf et al., 2011b) [B)] |
| Moosdorf4 | 110001 | Hydrosheds | Rocky Mountains | 134 | (Moosdorf et al., 2011b) [C)] |
| Moosdorf5 | 110006 | Hydrosheds | Rocky Mountains | 49 | (Moosdorf et al., 2011b) [C)] |
| Moosdorf6 | 110009 | Hydrosheds | Rocky Mountains | 98 | (Moosdorf et al., 2011b) [C)] |
| Moosdorf7 | 110052 | Hydrosheds | Rocky Mountains | 51 | (Moosdorf et al., 2011b) [C)] |
| Moosdorf8 | 110056 | Hydrosheds | Rocky Mountains | 50 | (Moosdorf et al., 2011b) [C)] |
| Moosdorf9 | 110059 | Hydrosheds | Rocky Mountains | 25 | (Moosdorf et al., 2011b) [C)] |
| Moosdorf10 | 110065 | Hydrosheds | Rocky Mountains | 49 | (Moosdorf et al., 2011b) [C)] |
| Pandey1 | Pindari Glacier | Hydrosheds | Himalaya | 4 | (Pandey et al., 2001) |
| Rainwater1 | Chamberlin Glacier | Hand | North | 20 | (Rainwater and Guy, 1961) |
| Reynolds1 | South Cascade Glacier | Hand | Rocky Mountains | 24 | (Reynolds and Johnson, 1972) |
| Rutter1 | Rieperbreen Svalbard USS | Aster | North | 16 | (Rutter et al., 2011) |
| Sharp1 | Haut d'Arolla Glacier | Hydrosheds | Alps | 300 | (Sharp et al., 1995) |
| Sharp2 | Robertson Glacier, RE Stream | Hand | Rocky Mountains | 12 | (Sharp et al., 2002) |
| Sharp3 | Robertson Glacier, RW Stream | Hand | Rocky Mountains | 12 | (Sharp et al., 2002) |
| Singh1 | Alaknanda, Station 1 | Hydrosheds | Himalaya | 1 | (Singh and Hasnain, 1998) |
| Singh2 | Gangotri Glacier, Garhwal Himalaya | Hydrosheds | Himalaya | 52 | (Singh et al., 2012) |
| Theakstone1 | Austre Oktsindbreen, Norway | Hand | North | 3000 | (Theakstone and Knudsen, 1996) |
| USGS1 | Andrews Creek | Hand | Rocky Mountains | 749 | (USGS, 2013)[D)] |
| USGS2 | Icy Brook | Hand | Rocky Mountains | 588 | (USGS, 2013)[D)] |
| Wadham1 | Finsterwalderbreen | Aster | North | 109 | (Wadham et al., 1998) |
| WolffBoehnisch1 | Nar (#2) | Hydrosheds | Himalaya | 16 | (Wolff-Boenisch et al., 2009) |
| WolffBoehnisch2 | Koto (#1) | Hydrosheds | Himalaya | 18 | (Wolff-Boenisch et al., 2009) |
| WolffBoehnisch3 | Upper Marsyandi (#4) | Hydrosheds | Himalaya | 17 | (Wolff-Boenisch et al., 2009) |
| WolffBoehnisch4 | Lower Marsyandi (#7) | Hydrosheds | Himalaya | 18 | (Wolff-Boenisch et al., 2009) |
| WolffBoehnisch5 | Dudh (#5) | Hydrosheds | Himalaya | 18 | (Wolff-Boenisch et al., 2009) |
| WolffBoehnisch6 | Dona (#6) | Hydrosheds | Himalaya | 18 | (Wolff-Boenisch et al., 2009) |
| WolffBoehnisch7 | Bhulbule (#8) | Hydrosheds | Himalaya | 19 | (Wolff-Boenisch et al., 2009) |
| Yde1 | Kuannersuit Valley | Hand | North | 134 | (Yde et al., 2005) |
| Yde2 | Longyearbreen | Aster | North | 183 | (Yde et al., 2008) |

| | | | | | |
|---|---|---|---|---|---|
| Yde3 | Austre Gronfjordbreen | Aster | North | 1 | (Yde et al., 2012) |
| Zhao1 | Site 1 | Hydrosheds | Himalaya | 13 | (Zhao et al., 2007) |

[1] method of catchment polygon generation: Hand -- hand-drawn catchment polygon based on satellite photographs and digital elevation models; Hydrosheds, Aster: Automatically generated catchments based on the respective DEM

[A)B)C)] Moosdorf et al. (2011b) are from previously compiled data; original data are from [A)] Alexander et al., 1996, [B)] Horowitz and Stephens, 2008, and [C)] Environment Canada, 2009

[D)] The Sr-isotope ratios (not used in this study, but in the compiled database) are from Clow et al., 1997

Table S2: Summary statistics for glaciated catchments by region, and comparison to literature values of global attributes.

| Attribute | Northern Latitudes | New Zealand | Alps | Himalaya | Rocky Mountains | Andes | Kilimanjaro | Iceland | Globe | Global comparison |
|---|---|---|---|---|---|---|---|---|---|---|
| Number of catchments | 20 | 13 | 8 | 18 | 18 | 10 | 1 | 7 | 95 | |
| Number of samples | 4241 | 35 | 638 | 568 | 2018 | 34 | 1 | 161 | 7696 | |
| Catchment area ($km^2$) | 82.6 | 231.2 | 26.1 | 702.7 | 3071.2 | 40.1 | 11.3 | 3137.9 | 1002 | |
| Glacial cover | 62.9% | 27.4% | 59.7% | 35.6% | 28.1% | 39.3% | 4.0% | 15.9% | 39.4% | 0.5% [A)] |
| Distance from snout (km) | 0.7 | 14.1 | 0.6 | 5.1 | 12.6 | 2.6 | 8.6 | 51.1 | 9.6 | |
| Ca conc. (µmol/L) | 179.6 | 235.9 | 72.1 | 429.2 | 320.8 | 502.5 | 22.3 | 74.7 | 276.9 | 374.3 [B)] |
| Mg conc. (µmol/L) | 71.6 | 27.2 | 11.4 | 174.9 | 103.4 | 210.2 | 12.6 | 40.3 | 97.7 | 168.7 [B)] |
| Na conc. (µmol/L) | 82.1 | 51.4 | 6.68 | 45.0 | 18.3 | 56.7 | 306.1 | 230.2 | 63.0 | 274.0 [B)] |
| K conc. (v) | 10.7 | 25.6 | 8.72 | 29.5 | 6.55 | 8.78 | 54.9 | 10.3 | 15.6 | 58.8 [B)] |
| Ca / cation flux (mol%) | 56.0% | 68.9% | 58.0% | 59.8% | 68.0% | 63.3% | 5.6% | 21.1% | 58.6% | 42.7% [B)] |
| Mg / cation flux (mol%) | 21.4% | 8.1% | 10.6% | 17.9% | 20.0% | 27.7% | 3.2% | 11.3% | 17.5% | 19.3% [B)] |
| Na / cation flux (mol%) | 18.9% | 15.9% | 14.8% | 11.3% | 7.9% | 7.7% | 77.3% | 64.7% | 17.4% | 31.3% [B)] |
| K / cation flux (mol%) | 3.7% | 7.2% | 16.6% | 11.0% | 4.1% | 1.3% | 13.9% | 2.9% | 6.5% | 6.7% [B)] |
| Carbonate-rich sed. | 58.9% | 29.4% | 14.0% | 7.8% | 25.8% | 50.0% | 0.0% | 0.0% | 29.2% | 25% [C)] |
| Siliciclastic sediment | 6.6% | 8.5% | 2.4% | 9.3% | 31.3% | 0.0% | 0.0% | 0.0% | 10.4% | 46.10% [C)] |
| Metamorphics | 27.7% | 61.6% | 33.1% | 59.2% | 22.0% | 0.0% | 0.0% | 0.0% | 32.4% | 14.5% [C)] |
| Volcanic rocks | 6.7% | 0.0% | 2.8% | 0.0% | 12.8% | 50.0% | 100.0% | 99.8% | 17.8% | 6.90% [C)] |
| Plutonic rocks | 0.2% | 0.5% | 47.7% | 23.7% | 8.0% | 0.0% | 0.0% | 0.2% | 10.1% | 7.50% [C)] |
| Catchments with flux data | 15 | 0 | 6 | 13 | 10 | 1 | 0 | 7 | 52 | |
| Runoff ($mm\ a^{-1}$) | 1090 | | 2401 | 1517 | 2162 | 2771 | | 2182 | 1733 | 300 [D)] |
| Weathering yield ($t\ km^{-2}\ a^{-1}$) | 14.70 | | 6.37 | 35.93 | 20.26 | 36.10 | | 21.13 | 21.39 | 10.7 [E)] |
| Ca yield ($10^6\ mol\ km^{-2}\ a^{-1}$) | 0.22 | | 0.11 | 0.66 | 0.40 | 0.72 | | 0.16 | 0.35 | |
| Mg yield ($10^6\ mol\ km^{-2}\ a^{-1}$) | 0.15 | | 0.01 | 0.27 | 0.11 | 0.14 | | 0.09 | 0.15 | |
| Na yield ($10^6\ mol\ km^{-2}\ a^{-1}$) | 0.09 | | 0.02 | 0.06 | 0.04 | 0.12 | | 0.50 | 0.12 | |
| K yield ($10^6\ mol\ km^{-2}\ a^{-1}$) | 0.01 | | 0.03 | 0.04 | 0.02 | 0.02 | | 0.02 | 0.02 | |

Comparison values from: [A)] Arendt et al., 2012; [B)] Livingstone, 1963; [C)] Hartmann and Moosdorf, 2012; [D)] Fekete et al., 2002; [E)] Hartmann et al., 2014
Weathering yields all reflect dissolved export from catchments

Table S3: Spearman rank correlations of different analyzed parameters.

| | $SO_4$ / $HCO_3$ | Glacial cover % | Distance snout (m) | Runoff (mm $a^{-1}$) | Temp (°C) | pH | Carbonate -rich | Siliciclastic sediment | Meta-morphic | Volcanic rocks | Plutonic rock |
|---|---|---|---|---|---|---|---|---|---|---|---|
| CCC (µmol/L) | **0.23** | **-0.27** | 0.20 | **-0.36** | -0.01 | **0.43** | **0.26** | -0.05 | **-0.24** | 0.03 | -0.10 |
| CWR (t $km^{-2}$ $a^{-1}$) | 0.06 | **-0.31** | **0.30** | **0.28** | -0.03 | 0.31 | -0.10 | 0.19 | -0.09 | 0.10 | 0.18 |
| Ca / cation conc. (mol%) | -0.05 | 0.10 | -0.08 | -0.17 | 0.02 | **0.36** | **0.25** | **0.27** | -0.02 | -0.19 | -0.12 |
| Mg / cation conc. (mol%) | 0.17 | -0.02 | 0.03 | **-0.44** | -0.02 | 0.04 | **0.40** | -0.15 | -0.19 | -0.11 | -0.12 |
| Na / cation conc. (mol%) | -0.04 | -0.20 | 0.11 | 0.26 | 0.11 | -0.16 | **-0.42** | -0.12 | 0.09 | **0.35** | 0.04 |
| K / cation conc. (mol%) | 0.08 | **0.30** | **-0.29** | 0.24 | -0.18 | **-0.38** | **-0.43** | -0.11 | **0.54** | -0.13 | 0.19 |
| Ca / cation flux (mol%) | -0.07 | 0.20 | -0.20 | -0.14 | -0.05 | 0.21 | 0.23 | **0.30** | 0.21 | **-0.45** | 0.03 |
| Mg / cation flux (mol%) | 0.08 | -0.21 | 0.13 | **-0.43** | 0.28 | **0.41** | **0.55** | -0.08 | 0.06 | **-0.28** | -0.12 |
| Na / cation flux (mol%) | 0.07 | -0.20 | 0.14 | 0.22 | 0.04 | -0.19 | **-0.37** | -0.21 | -0.26 | **0.57** | -0.10 |
| K / cation flux (mol%) | **0.29** | **0.37** | **-0.43** | 0.22 | -0.12 | **-0.81** | **-0.44** | -0.13 | **0.29** | -0.12 | 0.06 |
| SO4 / anion conc. (mol%) | **0.98** | 0.13 | **-0.42** | -0.17 | **-0.44** | -0.09 | -0.02 | -0.09 | 0.13 | -0.22 | 0.04 |
| NO3 / anion conc. (mol%) | **0.29** | 0.11 | -0.10 | **0.35** | -0.21 | **-0.45** | **-0.43** | 0.07 | 0.06 | 0.16 | **0.44** |
| HCO3 / anion conc. (mol%) | **-0.82** | -0.15 | **0.28** | 0.10 | **0.42** | **0.42** | 0.22 | **0.27** | 0.00 | -0.08 | -0.06 |
| SO4 / anion flux (mol%) | **0.90** | 0.01 | **-0.39** | -0.16 | **-0.41** | **-0.39** | -0.02 | 0.05 | **0.40** | **-0.54** | 0.25 |
| NO3 / anion flux (mol%) | **0.40** | 0.09 | **-0.40** | **0.32** | 0.00 | **-0.49** | -0.28 | 0.27 | **0.36** | -0.22 | **0.34** |
| HCO3 / anion flux (mol%) | **-0.74** | -0.04 | **0.31** | 0.07 | **0.39** | **0.55** | 0.15 | 0.16 | -0.19 | 0.21 | -0.11 |
| SO4 / HCO3 (equivalent) | 1.00 | 0.07 | **-0.36** | -0.07 | **-0.45** | -0.19 | -0.17 | -0.06 | 0.12 | -0.12 | 0.11 |
| Glacial cover (%) | 0.07 | 1.00 | **-0.74** | 0.06 | **-0.68** | **-0.32** | 0.14 | **-0.35** | 0.12 | **-0.29** | **-0.21** |
| Distance from snout (m) | **-0.36** | **-0.74** | 1.00 | -0.04 | **0.45** | 0.24 | -0.14 | **0.33** | -0.08 | **0.36** | 0.18 |
| runoff (mm/a) | -0.07 | 0.06 | -0.04 | 1.00 | -0.05 | -0.22 | **-0.63** | 0.23 | -0.05 | **0.41** | 0.25 |
| Temp (°C) | **-0.45** | **-0.68** | **0.45** | -0.05 | 1.00 | 0.21 | 0.13 | **0.37** | -0.14 | 0.26 | -0.19 |
| pH | -0.19 | **-0.32** | 0.24 | -0.22 | 0.21 | 1.00 | 0.16 | **0.29** | -0.14 | 0.16 | -0.17 |
| Carbonate Sed. | -0.17 | 0.14 | -0.14 | **-0.63** | 0.13 | 0.16 | 1.00 | -0.06 | **-0.37** | **-0.38** | **-0.36** |
| Siliciclastic Sed. | -0.06 | **-0.35** | **0.33** | 0.23 | **0.37** | **0.29** | -0.06 | 1.00 | -0.07 | 0.01 | **0.20** |
| Metamorphic | 0.12 | 0.12 | -0.08 | -0.05 | -0.14 | -0.14 | **-0.37** | -0.07 | 1.00 | **-0.40** | 0.20 |
| Volcanic | -0.12 | **-0.29** | **0.36** | **0.41** | 0.26 | 0.16 | **-0.38** | 0.01 | **-0.40** | 1.00 | 0.03 |
| Plutonic | 0.11 | **-0.21** | 0.18 | 0.25 | -0.19 | -0.17 | **-0.36** | **0.20** | 0.20 | 0.03 | 1.00 |

**Bold**: significant correlations ($p<0.05$). Number of available pairs differs for each combination, with minimum n=27 (for runoff vs. pH)

Table S4: Ranges of end-member values used in inversion model to determine source contributions

| | Ca/Na | Mg/Na | Cl/Na | SO4/Na |
|---|---|---|---|---|
| silicate | 0.1-1 | 0.1-0.6 | 0 | * |
| carbonate | 30-70 | 12-28 | 0 | * |
| evaporite | 0.01-2 | 0.01-0.03 | 1 | 0.01-2 |
| rain | 0.02 | 15 | 0.5-2.5 | 0.1-13 |

* determined by inversion